Article

Spin-selective strong light–matter coupling in a 2D hole gas-microcavity system

In the format provided by the authors and unedited

CONTENTS

1. Spin selection rules for optical transitions

A fundamental condition, necessary for the spin-selective strong coupling reported in this work, is the existence of spin-selection rules that determine the optical transitions that can take place in the system. In this section, we will discuss the nature and origin of these selection rules, mostly based on Ref. [1]. They originate from the dipolar nature of the light-matter interaction which in turn arises from the spin conservation in photoabsorption events. Due to the strong spin-orbit coupling, the valence band (VB) energy is non-degenerate in quantum wells with a Zincblende crystalline structure. The VBs are composed of a band with a total angular momentum $J_z^h = \pm 3/2$ usually referred to as the "heavy-hole" (HH) band and one with $J_z^h = \pm 1/2$, referred to as "light-hole" (LH) band. It is the relative orientation of the spin and the orbital angular momentum which determines the nature of the hole band. In typical GaAs structures, the HH band is closer to the conduction band (CB) than the LH band, hence, in this analysis, we focus on the lowest energy optical transitions, i.e. those between the HH band and the CB.

The optical transition has a total angular momentum projection corresponding to the projection of the addition of angular momentum of electron ($J_z^e = \pm 1/2$) and HH ($J_z^h = \pm 3/2$). This transition can then have projections of the total angular momentum $J_z^T = \pm 1, \pm 2$. The angular momentum conservation implies that only those transitions matching the photon's angular momentum ± 1 can take place, hence, only the configurations in which the projections of electron and hole are anti-parallel are optically allowed. Typically, for a neutral QW system, the exciton corresponding to this projection is called "bright" exciton, in contrast to the $J_z^T = \pm 2$ case, referred to as "dark" exciton.

These selection rules determine the existence of spin selectivity in the strong coupling. Figure S1 shows a diagram of the optical selection rules. It shows how the transition from the spin up (down) VB to the spin up (down) CB is optically forbidden, which justifies why
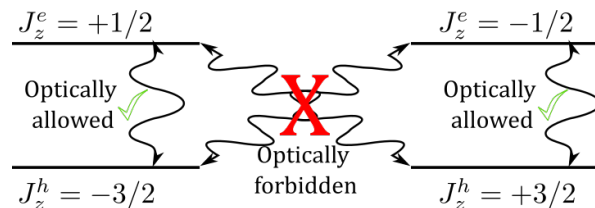

FIG. S1. Optical selection rules for a GaAs quantum well for transitions between the HH band and the CB.

these transitions are not indicated in Fig. 1b-d of the main document.

2. Hole density calibration

At a temperature of 40 mK, the hole gas is capable of sustaining correlated states of matter at integer filling fractions. As mentioned in the main text, this result has been previously reported [2]. This gives a very accurate method for calibrating the hole density: since the magnetic field strength and the gate voltage are known quantities, one can infer the hole density from the optical signatures of the integer filling factor states $\nu = 1$ or $\nu = 2$. According to quantum Hall physics, these correlated states are established when $\rho h/eB \in \mathbb{Z}$. Depending on ρ, one can observe both correlated states, one of them, or none. This limitation is imposed by the finite hole mobility in the sample. Figure S2 shows the reflectivity spectrum of the system at low numerical apertures i.e. close to zero in-plane momentum, as a function of the magnetic field. After systematically collecting data for different gate voltages, and recording the magnetic fields at which the Rabi splitting is modified, one can obtain an accurate linear model that gives the hole density of the system as a function of the gate voltage.

The density is not perfectly uniform across the sample; we performed this calibration in different spots obtaining different results. For this reason, it is important to perform a calibration procedure every time the position of the excitation spot on the sample changes. Figure S3 shows the deduced hole density for each given gate voltage at a given spot of the sample. The procedure consists in registering the magnetic field at which the Rabi splitting is modulated for a given gate voltage. With this information, we infer the hole density according to the formula $\rho = eB\nu/h$. ν taking the values 1 or 2. Notice from the figure that for some gate voltages both integer filling fractions are displayed, because in those cases the optical signatures of both states are observable. This corresponds, for example, to the case displayed in Fig. S2a. For other gate voltages, only one of the correlated states can be detected as shown, for example, in Fig S2b. However, for very high or very low densities, none of the correlated states can be observed (Fig. S2c).
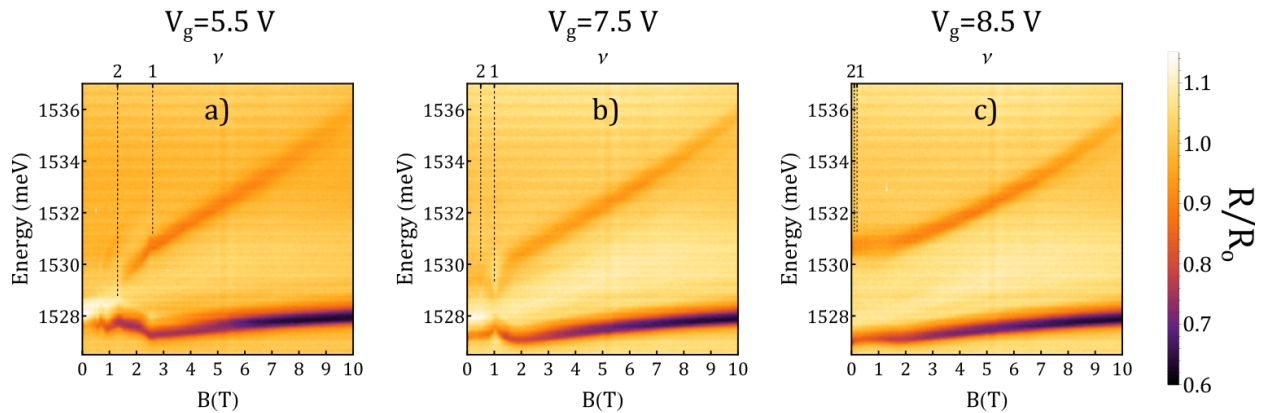
FIG. S2. Differential reflectivity of the system at 40 mK. The displayed data corresponds to low numerical apertures ($k \sim 0$). The gate voltage sets the hole density and a sweep over the magnetic field allows us to identify the correlated states of matter associated with integer filling fractions. Due to the finite hole mobility of the sample, the effect is not visible for every density. In the figure, one can observe that for high densities, the modification of the absorption spectrum corresponding to $\nu = 1$ and $\nu = 2$ can be observed (panel a). For medium densities, only $\nu = 1$ shows the feature (panel b) and for low densities, none of the correlated states is observable (panel c). The top axis indicates the magnetic fields corresponding to integer filling fractions obtained from an interpolation of the results.

After recording the calculated density for each gate voltage, we use the best-fitting linear function as a reference for the system's density once the temperature is increased from 40 mK to 3.5 K. Finally, it is worth mentioning that we did not detect any optical signal related to fractional quantum Hall states in the full range of charge density. The formation of these states requires very high charge mobility (μ). For example, the reported fractional states in polaritonic microcavities [3] were achieved in a system with $\mu = 1.6 \cdot 10^6$ cm^{2}V^{-1}s^{-1}, which according to our characterization, is at least 5 times higher than the mobility of the sample employed in the present work.
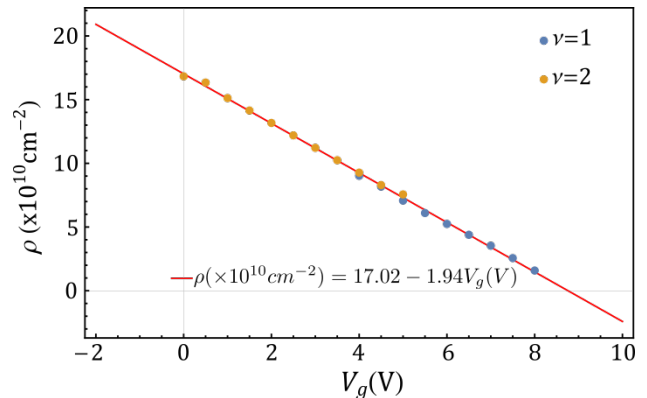

FIG. S3. Voltage to hole density calibration. From the low momentum reflectivity spectrum, we extract the values of the magnetic fields for which the correlated states of matter take place for each voltage. In some cases both ($\nu = 1$ and $\nu = 2$) states are observable, in some cases only one of them is, and for very high and very low densities, none of the correlated states are observable. The red line shows the fitting line for the data set, which we use as a reference to obtain the hole density at 3.5 K. The range of the horizontal axis corresponds to the range at which we collected data.

3. Comparison of the system response at T=40mK vs T=3.5K

In this section we discuss the fundamentally different response of the physical system when probed at 40 mK or 3.5 K. This is important because the previously reported modulation of the Rabi splitting [2–4] relies on correlated states of matter that can only take place at these ultra-cold temperatures, while the effect we exploit to induce the spin-selective strong coupling does not rely on this physics. As mentioned in the main text, the optical features from the correlated states at integer filling fractions are completely washed out when the temperature is 3.5 K. A magnetic field dependence was collected in identical conditions at 40 mK and 3.5 K for two densities: ($9.4 \cdot 10^{10} cm^{-2}$ and $6.88 \cdot 10^{10} cm^{-2}$). The results, displayed in Fig. S4 respond to the difference of the reflectivity spectra for σ^+ and σ^- polarization

collected with low numerical aperture. The subtraction of the reflectivity spectra allows us to show both of the spin (polarization) states in a single frame. In contraposition with the data presented in Fig. 3 of the main text, the in-plane momentum is constant over this set of data ($k \sim 0$).

Figure S4 features a much richer behavior at a temperature of 40mK with respect to the 3.5K case. For example, at specific values of the magnetic field,
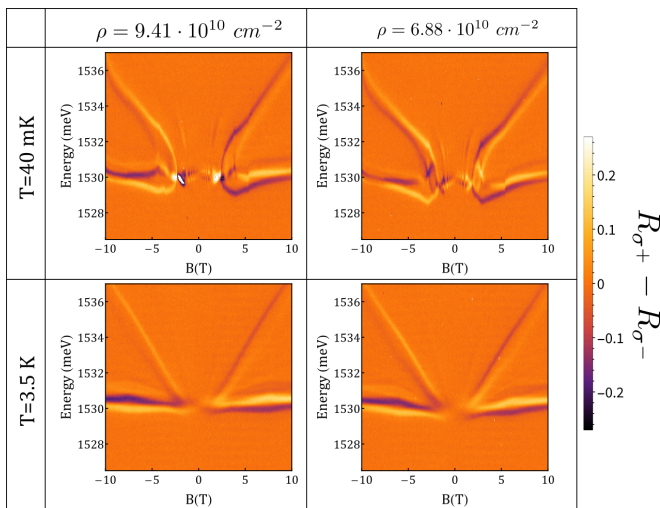
FIG. S4. Difference of the reflectivity spectra for the two circular states of polarization. The data is presented for two densities ($9.41 \cdot 10^{10}$cm^{-2} and $6.88 \cdot 10^{10}$cm^{-2}) and for two temperatures (40 mK and 3.5 K). The modulation of the resonance energy peak associated with correlated states of matter is visible only for the data collected at the dilution unit base temperature (40 mK).

the Rabi splitting is strongly modified. While the overall splitting of different polarization branches can be understood using our single-particle picture, presented in the main text, the finer features require more investigation. Generally, one can associate such features with Coulomb interaction in creating correlations at such low temperatures. For example, at $\nu = 1$, certain skyrmion physics can be observed similar to ETHZ earlier work [2]. At mK temperatures, the thermal energy is low enough to allow the establishment of these Coulomb-induced correlations that go beyond the Pauli exclusion. On the other hand, at higher temperatures (3.5 K, shown in the lower panels of Fig. S4), the thermal excitations have enough energy to bring the system into excited states, which consist of the delocalization of the charges and the destruction of the spin order. As pointed out in the main text, the spin selectivity reported in this work does not rely on the Coulomb-induced spin order but its robustness depends on the high Zeeman splitting between Landau levels with opposite spin.

There are two energies that, when compared with T, determine the ground state of the system: the Coulomb interaction and the Zeeman splitting between Landau Levels. In the previous paragraph, we established that at 3.5 K, the thermal fluctuations destroy the localization and magnetization induced by charge repulsion, for which we will focus now on the second quantity: Zeeman splitting vs T. For a system following the Fermi-Dirac distribution, one would expect T to attempt against the spin selectivity by inducing thermal transitions in the

hole gas. In this scenario, the holes population in the σ^- level could be excited to the σ^+ level; or in other words, T would induce electronic transitions from σ^+ to σ^-. The consequence would be the loss of spin selectivity because now both bands would have available electrons to perform an optical transition. Although we can't measure the band structure of the system, the robustness of the effect indicates that the energy splitting between the σ^+ and σ^- levels is higher than the thermal energy (T= 0.3 meV at 3.5 K). This allows us to neglect the effect of T in our description. It is important to mention that the energy of the Landau levels of the valence band has a nontrivial dependence on both the magnetic field and the charge density, as it can be observed in reference [5]. Therefore, the energy splitting between the spin sub-bands cannot be easily estimated.

4. Details on the theoretical formalism for data fitting

The coupled oscillators formalism employed for the theoretical modelization of the polaritonic system is described by the Hamiltonian

$$\hat{H} = \sum_k \left(\omega_c + \frac{k^2}{2m} \right) \hat{a}_k^\dagger \hat{a}_k + \omega_X(B) \sum_k \hat{b}_k^\dagger \hat{b}_k + \Omega(B) \sum_k (\hat{b}_k^\dagger \hat{a}_k + \hat{b}_k \hat{a}_k^\dagger) \tag{1}$$

As specified in the main text, ω_c is the cavity mode's energy, k its momentum, m its effective mass, and $\omega_X(B)$ and $\Omega(B)$ are the energy of the electronic transition and the Rabi splitting, respectively [1]. Once collected, we fit the data by using ω_X and Ω as fitting parameters for each magnetic field. The data is then fitted to the eigenfunctions of the hamiltonian 1, which are given by:

$$E_{U/L} = \frac{1}{2} \left(\omega_X + \omega_c + \frac{k^2}{2m} \right) \pm \frac{1}{2} \sqrt{\Delta_k^2 + 4\Omega^2} \tag{2}$$

With $\Delta_k = \omega_c + \frac{k^2}{2m} - \omega_X$. The cavity's energy and effective mass is accurately extracted from the case $\Omega = 0$ since in this condition, only the bare cavity mode is visible. For the mass, we obtain the value m = $2.4 \cdot 10^{-5}$m$_e$, with m$_e$ the free electron mass. This value is kept constant over the fitting procedure of the full data set and it is consistent with typical values for these devices. The cavity energy accounts only for minor changes due to the response of the optical properties of the bare electromagnetic mode to the high magnetic and electric fields. In the absence of any field, the cavity mode at 0 in-plane momentum has energy $\omega_C = 1530$ meV, and for the full set of data (0V to 10V and -10T to 10T), it never changes by more than 0.5 meV.

This model accurately reproduces the experimental data as it can be observed in the Supplementary videos, which show the evolution of the far-field reflectivity with

an increasing magnetic field for different hole densities. The main document also displays one fitted set of data in Fig. 2f.

———

[1] A. V. Kavokin, J. J. Baumberg, G. Malpuech, and F. P. Laussy, *Microcavities* (Oxford University Press, 2017).
[2] M. Lupatini, P. Knüppel, S. Faelt, R. Winkler, M. Shayegan, A. Imamoglu, and W. Wegscheider, Phys. Rev. Lett. **125**, 067404 (2020).
[3] S. Ravets, P. Knüppel, S. Faelt, O. Cotlet, M. Kroner, W. Wegscheider, and A. Imamoglu, Phys. Rev. Lett. **120**, 057401 (2018).
[4] S. Smolka, W. Wuester, F. Haupt, S. Faelt, W. Wegscheider, and A. Imamoglu, Science **346**, 332 (2014).
[5] M. K. Ma, C. Wang, Y. J. Chung, L. N. Pfeiffer, K. W. West, K. W. Baldwin, R. Winkler, and M. Shayegan, Phys. Rev. Lett. **129** (2022).